ADVANCES IN ATMOSPHERIC SCIENCES, VOL. 29, NO. 2, 2012, 236–248

Development of Cloud Detection Methods Using CFH, GTS1, and RS80 Radiosondes

ZHANG Jinqiang[1] (张金强), CHEN Hongbin*[1] (陈洪滨), BIAN Jianchun[1] (卞建春), XUAN Yuejian[1] (宣越健), DUAN Yunjun[2] (段云俊), and Maureen CRIBB[3]

[1] *Key Laboratory of Middle Atmosphere and Global Environment Observation, Institute of Atmospheric Physics, Chinese Academy of Sciences, Beijing* 100029

[2] *Kunming National Reference Climatological Station, Kunming* 650034

[3] *Department of Atmospheric and Oceanic Science and Earth System Science Interdisciplinary Center, University of Maryland, College Park, Maryland, USA*

(Received 10 June 2011; revised 20 September 2011)

ABSTRACT

The accuracies of three instruments in measuring atmospheric column humidity were assessed during an upper troposphere and lower stratosphere observation campaign conducted from 7 to 13 August 2009 in Kunming, China. The three instruments are a cryogenic frost-point hygrometer (CFH), a Vaisala RS80 radiosonde (RS80), and a GTS1 radiosonde (GTS1). The accuracy of relative humidity (RH) measurements made by the CFH, GTS1, and RS80 was similar between the surface and 500 hPa (∼5.5 km above sea level). However, above 500 hPa, the errors in RH measurements made by the RS80, relative to measurements made by the CFH, are much less than those detected with the GTS1. Three different retrieval methods for determining cloud boundaries from CFH, RS80, and GTS1 measurements were developed and take into account the differences in accuracy among the three instruments. The method for the CFH is based on RH thresholds at all levels, which demands high accuracy. Given that the accuracy of RH measurements decreases at higher altitudes, the cloud detection methods for RS80 and GTS1 are different for different altitude ranges. Below 5 km, the methods for the RS80 and the GTS1 are similar to that of the CFH; above 5 km, the methods for the RS80 and the GTS1 are both developed based on the second-order derivatives of temperature and RH with respect to height, but with different criteria applied. Comparisons of cloud-layer retrievals derived from the three measurements are also made.

Key words: CFH, GTS1, RS80, cloud vertical structure, detection

Citation: Zhang, J. Q., H. B. Chen, J. C. Bian , Y. J. Xuan, Y. J. Duan, and M. Cribb, 2012: Development of cloud detection methods using CFH, GTS1, and RS80 radiosondes. *Adv. Atmos. Sci.*, **29**(2), 236–248, doi: 10.1007/s00376-011-0215-4.

1. Introduction

Cloud vertical structure and the distribution of multi-layered clouds within the atmosphere affect atmospheric dynamics, thermodynamics, and the hydrological cycle, as well as incoming solar and outgoing thermal radiation (Chahine et al., 2006). Validation of climate models requires accurate basic cloud information, such as cloud-base height, cloud-top height, and cloud thickness from observational data. Radiosondes can provide in-situ measurements of vertical profiles of temperature, relative humidity (RH), and pressure inside clouds, which are fundamental to the study of atmospheric thermodynamic and dynamic processes.

Radiosondes with high vertical resolution have been widely used to obtain atmospheric parameters, including those of cloud vertical structure. Methods have been developed to determine locations of cloud layers and their boundaries from radiosonde measurements (Arabey, 1975; AWS, 1979; Dolgin, 1983; Wang

*Corresponding author: CHEN Hongbin, chb@mail.iap.ac.cn

and Sheng, 1991; Xu, 2006). Poore et al. (1995; hereafter PWR95) used rawinsonde observations to determine the boundaries of cloud layers by testing dew point temperature depressions below some threshold values. Wang and Rossow (1995; hereafter WR95) used RH profiles to obtain cloud vertical structure with a transformation of RH with respect to ice at levels where the temperature is below 0°C. In WR95, the cloud base and top locations were identified using the following criteria: maximum RH ($\mathrm{RH_{max}}$)>87%; minimum RH ($\mathrm{RH_{min}}$)>84%; a RH jump ($\mathrm{RH_{jump}}$) of $\geqslant$3% from the cloud base or cloud top to the immediate level below or above, respectively. The cloud base of the lowest layer of cloud was set at 500 m above ground level (AGL). Note that these RH thresholds were modified from 87% to 93% and from 84% to 90% in the analysis of cloud vertical structure at Porto Santo Island (Wang et al., 1999). Chernykh and Eskridge (1996; hereafter CE96) developed a cloud detection method based on $T''(z)$ and $\mathrm{RH}''(z)$, which are the second-order derivatives of temperature and relative humidity with respect to height, respectively. Criteria for retrieving a cloud layer are $0 \leqslant T^{''}(z)$ and $\mathrm{RH}^{''}(z) \leqslant 0$. Cloud boundaries are defined where at least one of the two second-order derivatives is zero. Cloud amount was further predicted in CE96 from a relationship between cloud amount and dew point depression within the predicted cloud layer and the temperature at that level, and it was divided into four categories: 0%–20%, 20%–60%, 60%–80%, and 80%–100% coverage.

Chernykh et al. (2000) analyzed trends in low and high cloud boundaries and their associated errors by using radiosonde data from 795 global stations. Minnis et al. (2005) made a comparison between RH and cloud cover from Vaisala RS80-15LH radiosonde observations and rapid update cycle (RUC) model simulations over the Department of Energy (DOE) Atmospheric Radiation Measurement (ARM) Southern Great Plains (SGP) Central Facility (SCF) site. They found that both types of data could be used to estimate the occurrence of clouds, although RS80 radiosonde data appeared to be more reliable than the RUC data. Naud et al. (2003) used lidar and ceilometer data collected at the SCF during November 1996 through October 2000 to assess the retrievals of the WR95 and the CE96. Cloud boundaries derived from cloud radar and radiosonde observations agreed better for cloud-base heights than for cloud-top heights; overall, the WR95 method tended to misclassify moist, cloud-free layers as clouds. Both radiosonde techniques reported higher cloud tops than those from the cloud radar, a result that is associated with the following factors: (1) sampling difference between the radiosonde- and ground-based observations; (2) the effects of precipitation on ground-based instruments; (3) the cutoff in range of the radar around 15 km, leading to a low bias in cloud top height; (4) attenuation of the radar beam; (5) insufficient radar sensitivity to detect cloud tops containing small particles; and (6) a slow recovery time of the radiosonde humidity sensor, leading to a high bias in cloud-top height.

From 7 to 13 August 2009, an upper troposphere and lower stratosphere (UTLS) observation campaign was conducted in Kunming, China. A cryogenic frost-point hygrometer (CFH), a Vaisala RS80 radiosonde (RS80), and a GTS1 radiosonde (GTS1) were deployed in the experiment. Based on relatively precise measurements from the CFH, Bian et al. (2011) analyzed the accuracy in RH from measurements made by the GTS1. Below 500 hPa, the average dry bias of GTS1 was on the order of 10% (similar to that of the Vaisala RS80); above 500 hPa, the dry bias of GTS1 jumped to 30% and increased rapidly to 55% at 310 hPa, while the RS80 showed a slowly dry bias. Temperature observations from the RS80 and the GTS1 agree well in the troposphere.

The goal of this study was to determine cloud-base and cloud-top locations from observations collected by the aforementioned instruments, based on the methods of WR95 and CE96. Because the RH accuracy is different for each instrument, cloud determining methods were modified according to their RH accuracies. Differences in cloud-layer locations derived from the three different instruments are also discussed.

Section 2 describes the instruments and data employed in this study. Methods for determining cloud vertical structure and results are presented in section 3. A discussion and summary are given in section 4.

2. Observations and data

The distribution of and long-term changes in water vapor within the UTLS plays an important role in climate change. Water vapor, as the most important greenhouse gas in the UTLS, not only has strong radiative forcing but also affects the microphysical and chemical processes within this region of the atmosphere (Chen et al., 2006; Bian, 2009). From 7 to 13 August 2009, an UTLS observation campaign was conducted in Kunming (25.01°N, 102.65°E, 1889 m above sea level), China. Its goal was to study water vapor and ozone distribution features in the UTLS during the Asian summer monsoon season. The water vapor content in the UTLS is too low to be well detected by routine operational radiosondes. The CFH, developed by the University of Colorado, is an instrument with high accuracy in detecting water vapor so it was adopted as the benchmark for such measure-

Table 1. Summary of the launches.

	Launch time		Burst altitude (km)	
Launch No.	GTS1	RS80/CFH	GTS1	RS80/CFH
1	–	20090807 14:02:05 A	–	33.11
2*	20090808 14:11:00	20090808 14:11:00 H	30.49	30.49
3*	20090809 14:02:24	20090809 14:02:24 A	31.15	31.15
4	20090809 19:15:47	20090809 19:04:02 A	33.28	33.72
5*	20090810 14:12:32	20090810 14:12:32 H	31.96	31.96
6	20090810 19:15:13	20090810 19:04:09 A	36.95	34.98
7*	20090811 14:06:10	20090811 14:06:10 A	33.15	33.15
8	20090811 19:15:28	20090811 19:02:41 H	37.90	33.82
9*	20090812 14:02:21	20090812 14:02:21 A	31.64	31.64
10*	20090813 13:59:41	20090813 13:59:41 H	32.57	32.57
11	20090813 19:15:17	20090813 19:31:30 A	5.92	31.92

Note: * indicates the same balloon launched with the GTS1 and the RS80/CFH; A and H represent the RS80 Vaisala humicap sensor type (A-humicap and H-humicap); − means that GTS1 is not available for Launch No. 1.

ments in this study. Notably, the CFH used in the experiment collected the first ever in-situ observations of water vapor in the UTLS during the Asian summer monsoon season. The Electrochemical Concentration Cell (ECC) ozondesonde (EnSci Co., USA) was used to measure ozone profiles. Temperature, RH, and pressure profiles were obtained using the RS80. A total of 11 sounding balloons were launched, with an average burst altitude of 32 km. To assess the performance of the GTS1, the instrument was also deployed in 10 of the 11 launches. Operational information about the launches is summarized in Table 1.

The CFH, whose operation is based on the chilled-mirror principle, is a balloon-borne hygrometer with the capability of continuously measuring water vapor from the surface to the middle stratosphere (Miloshevich et al., 2001; Vömel et al., 2007a). A small mirror is electrically heated against a cryogenic cold sink to maintain a constant layer of condensate that is optically detected. The mirror temperature is equal to the ambient dew point temperature (T_d) when the condensate phase is liquid or the frost-point temperature (T_f) if the condensate is ice. To remove ambiguity as to the water phase on the mirror, the liquid layer is forced to freeze by briefly cooling the mirror to -40°C when T_d first reaches -15°C, thereby guaranteeing that T_f is measured thereafter (Miloshevich et al., 2009). The water vapor mixing ratio and RH can be calculated using the Clausius–Clapeyron equation. The air temperature is measured by an attached RS80 radiosonde, and the saturation water vapor pressure is calculated using the Hyland and Wexler (1983) formulation which is implicitly employed in the Vaisala radiosonde calibration procedure. The CFH uses a Vaisala RS80 radiosonde as the data transmitter. The measurement uncertainty of RH from the CFH was estimated by Vömel et al. (2007a), and ranged from <4% in the tropical lower troposphere to ⩽10% in the middle stratosphere at 28 km; the uncertainty was <9% in the tropopause region.

An L-band (1675 MHz) electronic sounding system (Shanghai Changwang Meteorological Science and Technology Company, China) replaced the old radiosonde system in operation until 2001. The L-band sounding system, composed of a secondary wind-finding radar, a GTS1 digital electronic radiosonde, and a ground-check set was used to measure the temperature, pressure, RH, and wind from the surface to ∼30 km (Li, 2006; Li et al., 2009). Compared to the old radiosonde system (radiosonde 57–701), the GTS1 performs better, but it still has a dry bias in RH measurements (Yao et al., 2008; Li et al., 2009). To be well shielded from the direct sunlight, the GTS1 carbon hygristor is located inside the duct (Bian et al., 2011). However, the entire air mass passing through the duct may be heated by the shield. So, the RH reading would be taken at a warmer temperature than that shown by the air temperature sensor, resulting in a lower RH.

The RS80 radiosonde measures temperature with a small, temperature-sensitive capacitor, consisting of two electrodes separated by a ceramic dielectric. The humidity is measured with Humicap technology which separates two electrodes with a thin polymer film. The RH detection error of the RS80 increases as the ambient temperature decreases (Miloshevich et al., 2001; Wang et al., 2003; Turner et al., 2003), with high accuracy in the low-to-middle troposphere but a dry bias in the upper tropospheric region.

3. Cloud detection methods using CFH, GTS1 and RS80 observations

Profiles of RH and temperature taken on 8 August 2009 by the three instruments launched on the same

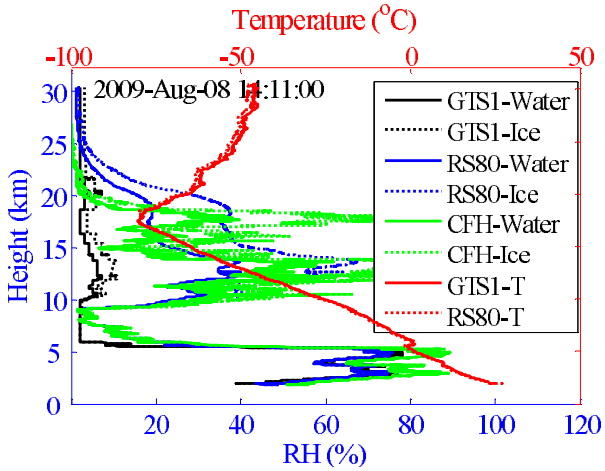

Fig. 1. Profiles of relative humidity (with respect to water and ice) measured by the CFH (in green), the GTS1 (in black), and the RS80 (in blue) and temperature measured by the GTS1 and the RS80 (in red) on 8 August 2009.

balloon are shown in Fig. 1. RH at all levels with temperatures below 0°C was transformed to that with respect to ice following the relation proposed by Alduchov and Eskridge (1996).

The RH profiles measured by the three instruments were similar below 5 km. Above 5 km, the RS80 can generally capture changes in RH, but with a noticeable dry bias; the GTS1 has a much larger dry bias. The temperature profiles from the GTS1 and the RS80 are in good agreement below 18 km. Above 18 km, the GTS1 records higher temperatures than the RS80. Therefore, due to these differences in measurement accuracy, different cloud-detection methods should be developed for each instrument. Criteria for determining cloud layers are different in the methods of WR95 and CE96. The WR95 method uses an RH threshold to retrieve cloud layers, requiring highly accurate RH observations. The CE96 method retrieves cloud layers by analyzing the vertical variations of RH and temperature so that the accuracy requirement for this method is not as high as in the WR95 method. However, to obtain the best results in cloud-boundary retrievals, the vertical resolution of the data should range between 300 m and 600 m (Chernykh et al., 2000) and should be $\geqslant$200 m in the free troposphere (Naud et al., 2003). So, in view of the measurement accuracies of different instruments and application conditions in the WR95 and CE96 methods, retrievals of cloud boundaries for the CFH at all altitudes, and for the GTS1 and the RS80 at altitudes below 5 km (hereafter method-1), were developed by modifying the WR95 method; the methods for the GTS1 and the RS80 above 5 km (hereafter method-2) were developed based on the CE96 method. Only cloud layers with bases lower than 18 km were studied.

Case 2 in Table 1, the first launch when all three instruments were deployed, illustrates the retrieval methods developed here. The mean locations of cloud layers derived from cases 2–11 in Table 1 are also then presented for comparison.

3.1 *Method for the CFH*

The WR95 method was modified to determine cloud vertical structure, using RH profiles from the CFH which has high vertical resolution. The first step of this method is to transform RH with respect to ice for temperatures < 0°C using the formula proposed by Alduchov and Eskridge (1996). The threshold of an $\mathrm{RH_{jump}} > 3\%$ at cloud base and cloud top used in the WR95 method can be easily satisfied because this method is based on radiosonde data with low vertical resolution. As stated in WR95, minor variations in cloud-base and cloud-top heights are induced when the RH jump changes from 3% to 0% or from 3% to 6%. CFH observations have a higher vertical resolution of ~10–15 m. An RH jump of 3% at cloud base and cloud top is difficult to determine within such a short distance. The limitation on minimum cloud thickness for low and middle-to-high clouds in PWR95 were $>$ 30.5 m and >61.0 m, respectively, but these limitations were abandoned in WR95. To reduce the possibility of misclassifying thin, clear, moist layers as clouds, the minimum thickness limitations used in PWR95 were used in this study. Low, middle, and high clouds were defined as follows: (1) low clouds were defined as having bases < 2 km; middle clouds were defined as having bases ranging from 2 km to 5 km; and high clouds were defined as having bases > 5 km. For scattered cumulus clouds, RH probably decreases when the CFH passes through a cloud gap; it is possible to misclassify a cloud layer of scattered clouds as multi-layer clouds using minimum RH thresholds (hereafter Min-RH) and maximum RH thresholds (hereafter Max-RH). In this method, to reduce this possibility, two layers of cloud are considered as a one-layered cloud if the distance between the two contiguous layers is < 300 m or the RH within this distance (hereafter Inter-RH) is slightly less than Min-RH.

The lowest cloud base limit of 500 m AGL in WR95 was derived for a particular location, which was not suitable for the Kunming observation site. The Kunming site lies beside Lake Dian, where stratus clouds with low base heights frequently occur. So, for this location the lowest cloud base was set to 100 m AGL in our analysis.

The WR95 method is able to detect virtually all low clouds, but over-detects low-level clouds by ~10%

more than the surface weather observations (Wang and Rossow, 1995; Wang, 1997). It misidentifies some cloud-free, moist layers as clouds, and it misses high and thin clouds by 5% (Wang, 1997). To overcome the problem of false detection near the surface, Wang et al. (1999) increased the RH thresholds from 84% to 90%, and from 87% to 93%. Naud et al. (2003) suspected that the cloud boundary results from WR95 might perform better if the RH thresholds were larger at low altitudes and smaller at high altitudes. Slingo (1980) defined different RH thresholds for low-, mid- and high-level clouds in a numerical model cloud parameterization. Chernykh (1999) found a decrease in RH at cloud base with increasing cloud height for all cloud layers. By analyzing laser ceilometer data together with radiosonde RH data at the SCF site under broken cloud field conditions, Han and Ellingson (2000) confirmed the same phenomenon as Chernykh (1999), at least up to heights of 2.5 km. To determine cloud boundaries more accurately, it is thus necessary to take into account the altitude dependence of RH at cloud boundaries. By modifying the method presented in WR95 and using height-resolving RH thresholds, the cloud vertical structures at Shouxian, Anhui Province, China were obtained from the Vaisala RS92 radiosonde data collected at the ARM mobile facility (AMF) deployment (AMF-China) from 14 May to 28 December 2008 (Zhang et al., 2010). The radiosonde cloud detection method was also evaluated and validated using surface active remote sensing observations. Results show that cloud layers retrieved using the two cloud methods agree well at AMF-China site, and that the RH-threshold-based cloud retrieval method can capture cloud vertical distributions well.

Radiosonde accuracy varies substantially as a function of RH, temperature, solar altitude angle, and different radiosonde types have different strengths and weaknesses in different realms of RH and temperature spaces (Miloshevich et al., 2006, 2009). Compared with other types of radiosondes, the detecting accuracy of the Vaisala RS92 radiosonde is high (Miloshevich et al., 2006). However, a dry bias in the Vaisala humidity sensor was also revealed, which was associated with solar radiation, temperature-dependent calibration, and chemical contamination (Wang et al., 2002; Turner et al., 2003; Soden et al., 2004, Miloshevich et al., 2004, 2006; Vömel et al., 2007b; Cady-Pereira et al., 2008). Taking the CFH data as the benchmark, many studies have evaluated the performance of the RS92 in detecting RH. By analyzing 12 soundings during the AIRS Water Vapor Experiment in October and November 2003 at SCF, Vömel et al. (2007a) pointed out that the mean difference in RH between CFH and RS92 was $< 3\%$ within the entire troposphere. Miloshevich et al. (2009) assessed the RH detecting accuracy of the RS92, and results during the nighttime showed that below 500 hPa, the average difference between the CFH and the RS92 for detecting 48%–99% RH was $< 3\%$ and sometimes close to 0%, and that above 500 hPa, it was generally $< 5\%$. They also found that the RH detecting bias of the RS92 decreased as the ambient RH increased.

Therefore, based upon the above analysis of the RH detecting differences between the CFH and the RS92 and the study of Zhang et al. (2010) during the AMF-China, the RH thresholds used to determine cloud layers for the CFH were set as follows: (1) from the surface to 2 km above mean sea level (MSL), the RH thresholds were set to those of the RS92 at the surface (used during the AMF-China); (2) from 2 km MSL to 8 km MSL, they were set to those of the RS92 from 0 km above ground level (AGL) to 6 km AGL (used during the AMF-China); (3) from 8 km MSL to 14 km MSL, they were set greater than that of the RS92 from 6 km AGL to 12 km AGL (used during the AMF-China) (i.e., the difference increases linearly with height, which is 5% RH larger for the CFH at 14 km MSL than that for the RS92 at 12 km AGL); (4) above 14 km MSL, the RH threshold was set to that at 14 km MSL.

Compared to the nighttime bias, the bias of the RS92 during the daytime was larger and was associated with solar radiation (Miloshevich et al., 2009). However, this solar-radiation-related RH bias within cloud layers accompanied by high RH is not as obvious as that within clear layers. We assume that the RH detecting differences of the RS92 and the CFH in cloud layers during the daytime is approximately equal to that during the nighttime. Therefore, all RH thresholds for the CFH during the daytime were set to the same values as those during the nighttime specified above. To this end, Min-RH, Max-RH, and Inter-RH were set to decrease linearly with height; their values are given in Table 2.

The modified cloud detection algorithm of method 1, using the height-resolving thresholds in Table 2, is

Table 2. Summary of height-resolving RH thresholds for the CFH.

Altitude range	Height-resolving RH thresholds		
(above sea level)	Min-RH	Max-RH	Inter-RH
< 2 km	92%	95%	84%
2–8 km	92%–88%	95%–90%	84%–78%
8–4 km	88%–80%	90%–85%	78%–75%
> 14 km	80%	85%	75%

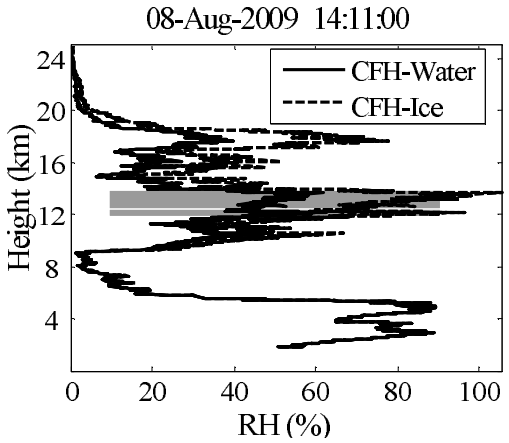

Fig. 2. Cloud layers derived from the RH profile measured by the CFH. The gray rectangles represent the locations of cloud layers. The solid and dotted lines show RH with respect to water and with respect to ice for levels with temperature $< 0°$C, respectively.

summarized as follows. Before applying any test, RH is first transformed with respect to ice for all levels with temperatures below 0°C. Then, RH is examined from the surface to upper levels to derive cloud layers in seven steps: (1) the base of the lowest moist layer is determined as the level with RH exceeding the Min-RH at this level; (2) above the base of the moist layer, contiguous levels with RH over the corresponding Min-RH are treated as the same layer; (3) the top of the moist layer is identified when RH decreases to a value below the corresponding Min-RH or when RH is over the corresponding Min-RH, but the top of the profile is reached; (4) the moist layer is classified as a cloud layer if the $\mathrm{RH_{max}}$ within this layer is greater than the corresponding Max-RH at the base of this moist layer; (5) the base of cloud layers starting at the ground is set to 100 m AGL and cloud layers are discarded if the cloud top is < 100 m; (6) two contiguous layers are considered as a one-layered cloud if the distance between these two layers is < 300 m or the $\mathrm{RH_{min}}$ within this distance is more than the maximum Inter-RH within this distance; and (7) cloud data are discarded if their thickness is < 30.5 m for low clouds, and < 61 m for middle-to-high clouds, and only cloud layers with bases <18 km are kept. Applying the modified method specified above, cloud layers derived for the case of the sounding launch No. 2 are shown in Fig. 2; two cloud layers were clearly detected.

3.2 *Method for the GTS1*

Below 5 km, the method of determining cloud layers from the GTS1 is similar to that for the CFH, and the RH is transformed with respect to ice for all levels with temperatures below 0°C. However, the average dry bias of the GTS1 is on the order of 10% below 500 hPa (Bian et al., 2011) and therefore Min-RH, Max-RH, and Inter-RH thresholds for the GTS1 are 10% RH less than the values used for the CFH. Given the large dry bias in measuring RH above 5 km, a new method to identify cloud layers in that part of the atmosphere is required. From now on, all the RH data used in section 3.2 were measured with respect to water.

The average ascending rate is $\sim$5 m s^{-1} for the GTS1 which takes measurements every 1–2 s, resulting in a high resolution of $\leqslant 10$ m (i.e., 5 m s^{-1} $\times$ 2 s). As mentioned previously, CE96 stated that the best cloud layer retrievals were obtained from observation data with low vertical resolution. So the data frequency from the GTS1 is reduced by first identifying four sets of heights from which subsets of data will be chosen: (1) from the surface upwards, at 600-m intervals; (2) at standard levels: 700, 500, 400, 300, 250, 200, 150, 100, 70, 50, 40, 20, 15 hPa, and at or near the thermodynamic first tropopause; and (3) the altitudes where extremes in RH or temperature (local minima or maxima) occur. Corresponding values of RH and temperature are selected at these various altitudes and then sorted according to ascending height from the surface. After processing, the average vertical resolution for cases 2–10 in Table 1 were 376 m, 268 m, 318 m, 264 m, 289 m, 315 m, 386 m, 330 m, and 281 m, respectively. The fitting curve was obtained by interpolating the selected data onto the altitudes of the original data.

The second-order derivatives of RH and temperature, $\mathrm{RH}''(z)$ and $T''(z)$, are shown in Fig. 3a. To clearly see the changes around the zero point of the x-axis, the x-axis in the figure ranges from -2 to 2. The corresponding results of cloud layers derived from the CE96 method are shown in Fig. 3b. Accurate RH measurements from the CFH are also shown in the figure.

Below 18 km, a total of 22 cloud layers were derived. Naud et al. (2003) used 4 years of radar, lidar and ceilometer data collected at the SCF site from November 1996 through October 2000 to assess the cloud-layer retrievals from the CE96 algorithm. They showed that some cloud layers with cloud amounts ranging from 60% to 100% derived from the CE96 were misidentified and were actually moist, cloudless layers. So it seems that the CE96 method identifies too many very thin cloud layers. There are two possible reasons for this: (1) many cloud-free layers with low RH were misidentified as cloud layers, and (2) one cloud layer was misclassified as multiple layers of cloud. More criteria must be applied to the measurements to avoid these kinds of misclassifications.

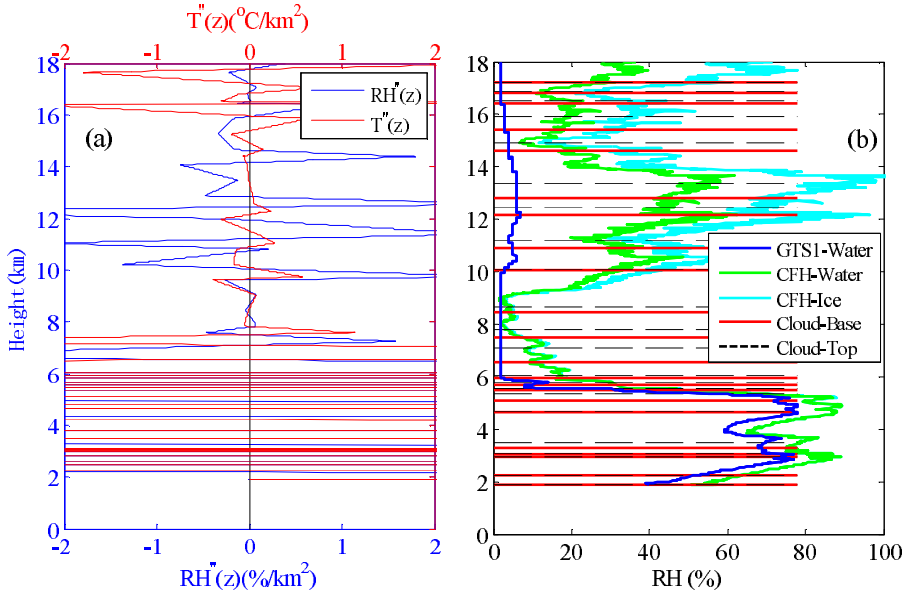

Fig. 3. The second-order derivatives of temperature and RH with respect to (a) height and (b) the cloud layers derived from CE96. The blue line represents RH with respect to water in GTS1 measurements; the green and cyan lines denote RH with respect to water and with respect to ice for levels with temperature $< 0°$C from CFH measurements; the red solid and black dotted lines illustrate the cloud base height and top height, respectively.

3.2.1 *Two contiguous cloud layers*

A preliminary scrutiny of the initial vertical distribution of cloud layers for each case is performed before applying further tests. Starting from the surface and working upwards, the distance between each consecutive pair of layers is assessed. If the distance between the layers is < 300 m, the layers are considered as one cloud layer and a check is made next of the distance between this new layer with the layer above, if it exists. This test proceeds up the atmospheric column until the topmost layer of cloud is reached.

Once this preliminary step is completed, further refinement in identifying contiguous cloud layers is made. The distance between two contiguous cloud layers is now defined as D, and the RH values within D are defined as $\mathrm{RH_{in}}$ The smaller of the values of RH at the base or the top of the lower layer of cloud is defined as $\mathrm{RH_1}$, and the larger one is defined as $\mathrm{RH_2}$. Because there is a decrease in RH at the cloud base as the cloud height increases, and if D is not too large, $\mathrm{RH_{in}}$ is compared to $\mathrm{RH_1}$. If the percentage of $\mathrm{RH_{in}}$ values greater than or equal to $\mathrm{RH_1}$ (hereafter, P) is large enough, two contiguous cloud layers are considered as one layer. The maximum value of D is set at 2.2 km. Because the dry bias in RH increases with rising altitude, P is set as a function of altitude: (1) Below 12 km, P is set at 70% because RH measurements can generally capture the varying trends. Two contiguous clouds with bases lower than 12 km, and satisfying the conditions that both $D \leqslant 2.2$ km and $P \geqslant 70\%$, are classified as one layer. (2) From 12 km to 15 km, there are large biases in RH, and sometimes there is little vertical variation of RH within this altitude range. P is set to 90% in this part of the atmospheric column. There is a distinct drop in RH from cloud layers into clear layers, so if the difference between $\mathrm{RH_2}$ and the maximum RH within D (hereafter, ΔRH) is $\geqslant 1\%$, there was a transition from a cloud layer to a clear layer. If two contiguous cloud layers with bases falling between 12 km to 15 km satisfy the conditions $D \leqslant 2.2$ km, $P \geqslant 90\%$, and $\Delta\mathrm{RH} < 1$, they are classified as one layer of cloud. (3) Above 15 km, there is less variation in RH, so ΔRH is set to $\leqslant 1\%$. Two contiguous layers with bases higher than 15 km and satisfying the conditions that $D \leqslant 2.2$ km, $P \geqslant 90\%$, and $\Delta\mathrm{RH} \leqslant 1$, are classified as one layer. A summary of the criteria for determining whether two contiguous layers can be classified as one layer is given in Table 3.

Table 3. Thresholds for combining two contiguous layers into one.

Altitude range	Criteria
5–12 km	$D \leqslant 2.2$ km and $P \geqslant 70\%$
12–15 km	$D \leqslant 2.2$ km, $P \geqslant 90\%$, and $\Delta\mathrm{RH} < 1$
> 15 km	$D \leqslant 2.2$ km, $P \geqslant 90\%$, and $\Delta\mathrm{RH} \leqslant 1$

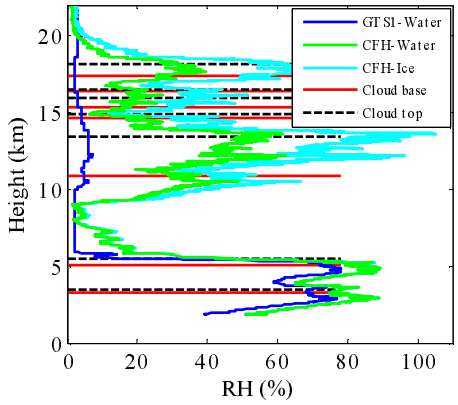

Fig. 4. Cloud layers derived from GTS1 measurements after application of additional criteria. All lines are the same as in Fig. 3b.

3.2.2 *Identification of other cloud layers from GTS1 measurements*

Below 7 km, RH measurements are relatively accurate. So for cloud layers with bases lower than 7 km, the $\mathrm{RH_{max}}$ within the layers must be >50%. Cloud layers with bases >18 km are discarded because these cloud types rarely occur. Middle and high clouds with thicknesses <61 m are also excluded.

Preliminary classification of cloud layers using the criteria introduced above are shown in Fig. 4. Agreement between the location of cloud layers from GTS1 and CFH measurements is better than that seen in Fig. 3b. However, at high altitudes, there are still discrepancies due to inaccurate RH measurements from the GTS1. If $D \leqslant 2.2$ km, $P \geqslant 90\%$, and $\Delta\mathrm{RH} \leqslant 1\%$for two contiguous layers with bases located between 12 km and 16 km, these layers are classified as one layer of cloud. Above 16 km, RH measurements are not accurate, so cloud layers with thicknesses <200 m are discarded.

3.3 *Method for the RS80*

First, the RH in this method is transformed with respect to ice for all levels with temperatures < 0°C. Below 5 km, method 1 is used to determine cloud layer boundaries from RS80 measurements (the same as those used for GTS1). Above 5 km, method 2, with some modifications particular to the RS80, was used to identify cloud boundaries.

The procedures for selecting original data and deriving cloud layers using $\mathrm{RH}''(z)$ and $T''(z)$ are the same as those used with GTS1 measurements. Further criteria that differ from those used with GTS1 measurements are introduced in the following subsections.

3.3.1 *Two contiguous cloud layers*

The variables D, $\mathrm{RH_{in}}$, P, $\mathrm{RH_1}$, and $\mathrm{RH_{max}}$ are the same as those defined in subsection 3.2. The $\mathrm{RH_{max}}$ at the top of lower cloud layer and the base of higher cloud layer of two contiguous cloud layers is defined as $\mathrm{RH_3}$.

The maximum value of D is set at 2.2 km. In the first condition, if $P \geqslant 70\%$, two contiguous cloud layers are classified as one layer. In the second condition, if $P < 70\%$, the maximum value of $\mathrm{RH_{in}}$ is compared to $\mathrm{RH_1}$. If their difference (hereafter, δ_{RH1}) is much greater than zero, then the layer with the larger RH is most likely a cloud layer. Therefore, provided that $\delta_{\mathrm{RH1}} \geqslant 12\%$ and $P \geqslant 45\%$, two contiguous cloud layers are classified as one layer of cloud. In summary, if $D \leqslant 2.2$ km, and either the first or second condition is satisfied, two contiguous cloud layers are identified as one cloud layer.

Because measurements of RH from the RS80 become less accurate with increasing altitude, further criteria that are a function of altitude are required to assess contiguous cloud layers.

Below 14 km, RH measurements are relatively accurate. For two contiguous cloud layers with bases located below 14 km, the maximum value of D is set at 2.2 km. In the first condition, if $P \geqslant 70\%$, $\mathrm{RH_3}$ is compared to the minimum value of $\mathrm{RH_{in}}$. If their difference (hereafter, $\delta_{\mathrm{RH_2}}$) is large, then the RH within D is small, so the layer is clear. Otherwise, there is little difference in the magnitude of RH within D and the two contiguous cloud layers, so D is thus considered as a cloud layer. The maximum value of $\delta_{\mathrm{RH_2}}$ is set at 12%. If $\delta_{\mathrm{RH_2}} \leqslant 12\%$, two contiguous cloud layers are classified as one layer of cloud. In the second condition, the difference between the maximum value of $\mathrm{RH_{in}}$ and $\mathrm{RH_3}$ is defined as $\delta_{\mathrm{RH_3}}$. A large value for $\delta_{\mathrm{RH_3}}$ signifies that compared to the two contiguous cloud layers, there are large values of RH within D. Values for $\delta_{\mathrm{RH_3}}$ are set to $> 8\%$. If $\delta_{\mathrm{RH_3}} > 8\%$, two contiguous cloud layers are classified as one layer. In summary, for cloud layers with bases below 14 km, if $D \leqslant 2.2$ km, and either condition (1) or (2) is satisfied, two contiguous cloud layers are identified as one cloud layer.

Above 14 km, the dry bias becomes larger. The maximum value of D is also set at 2.2 km. Two contiguous cloud layers are considered as one layer if $P \geqslant 70\%$ or $\delta_{\mathrm{RH_1}} \geqslant 12\%$.

3.3.2 *Identification of other cloud layers from RS80 measurements*

For cloud layers with bases below 11 km, $\mathrm{RH_{max}}$ must be $\geqslant 60\%$, and for cloud layers with bases between 11 km and 12 km, $\mathrm{RH_{max}}$ must be $\geqslant 50\%$. Two

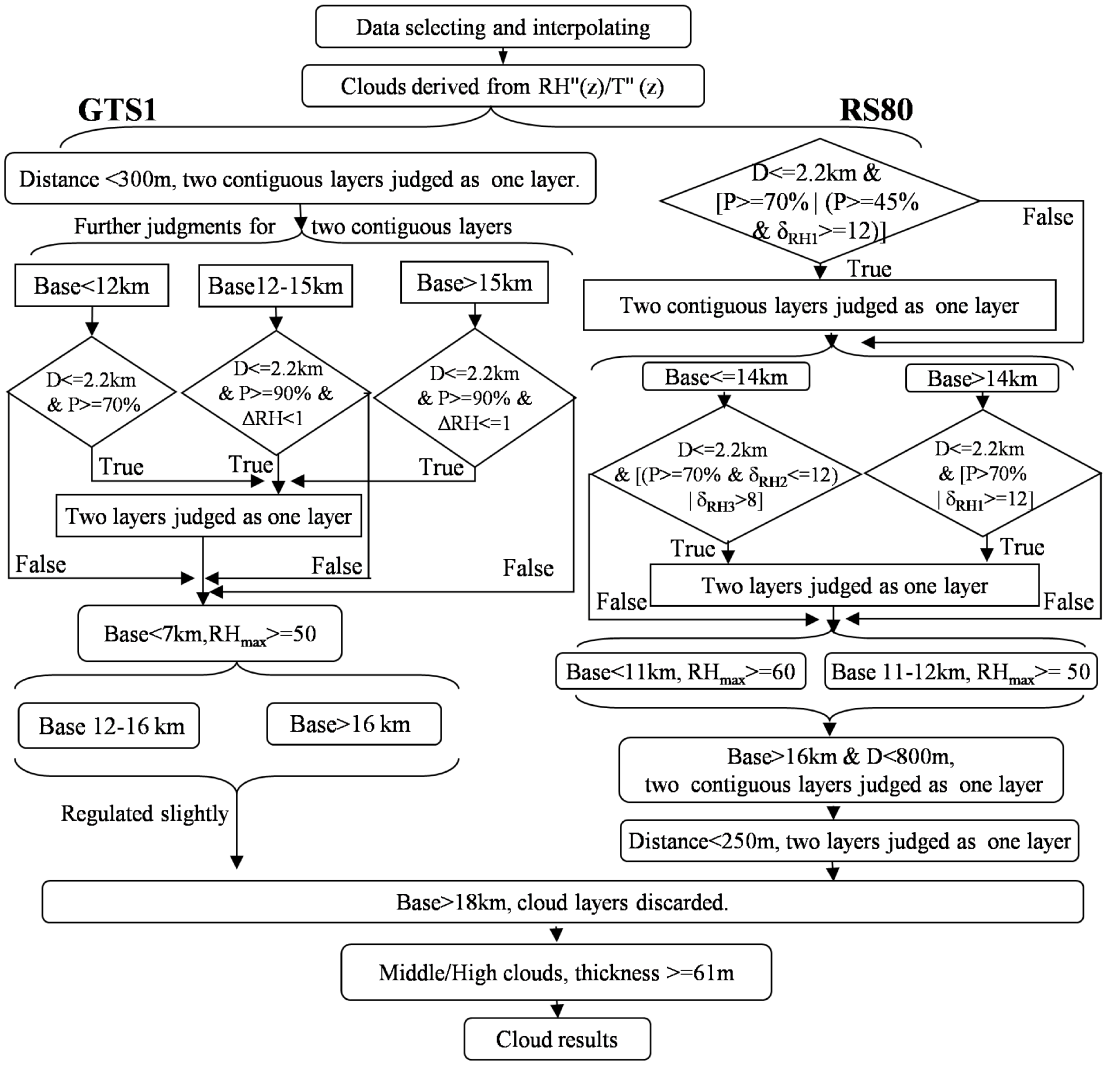

Fig. 5. Flowchart describing the steps in method-2 for determining cloud layer boundaries from GTS1 and RS80 measurements.

contiguous cloud layers with bases located between 16 km and 18 km are considered as one layer if the distance between them is < 800 m. Cloud layers with bases higher than 18 km are discarded. The thicknesses of middle and high clouds must be $\geqslant 61$ m.

Figure 5 shows the flowchart summarizing the steps in method 2 that were used to determine cloud layer boundaries from GTS1 and RS80 measurements.

3.4 *Comparison of cloud detection results*

Cloud layers retrieved using the methods described above applied to measurements made by the CFH, the GTS1, and the RS80 on 8 August 2009 at 1411 LST, case 2 described in Table 1, are shown in Fig. 6a. The numbers of cloud layers obtained by the CFH, the GTS1, and the RS80 are two, four, and four, respectively. The second highest cloud layer obtained from GTS1 and RS80 measurements is classified as two layers using CFH measurements. The lowest, third, and fourth cloud layers retrieved from the GTS1 and the RS80 are classified as cloud-free layers by the CFH; however, they generally correspond to moist layers with high RH in CFH observations. The second layer of cloud from the surface retrieved from RS80 measurements is thicker than that obtained by the GTS1, and the third layer of cloud is lower and much thinner than the third layer of cloud retrieved from GTS1 measurements. Overall, although differences exist for this particular case, all three instruments can provide reasonable information about the location of cloud layers or moist layers. Cloud layers retrieved from another launch, case 3 in Table 1 followed the above case 2,

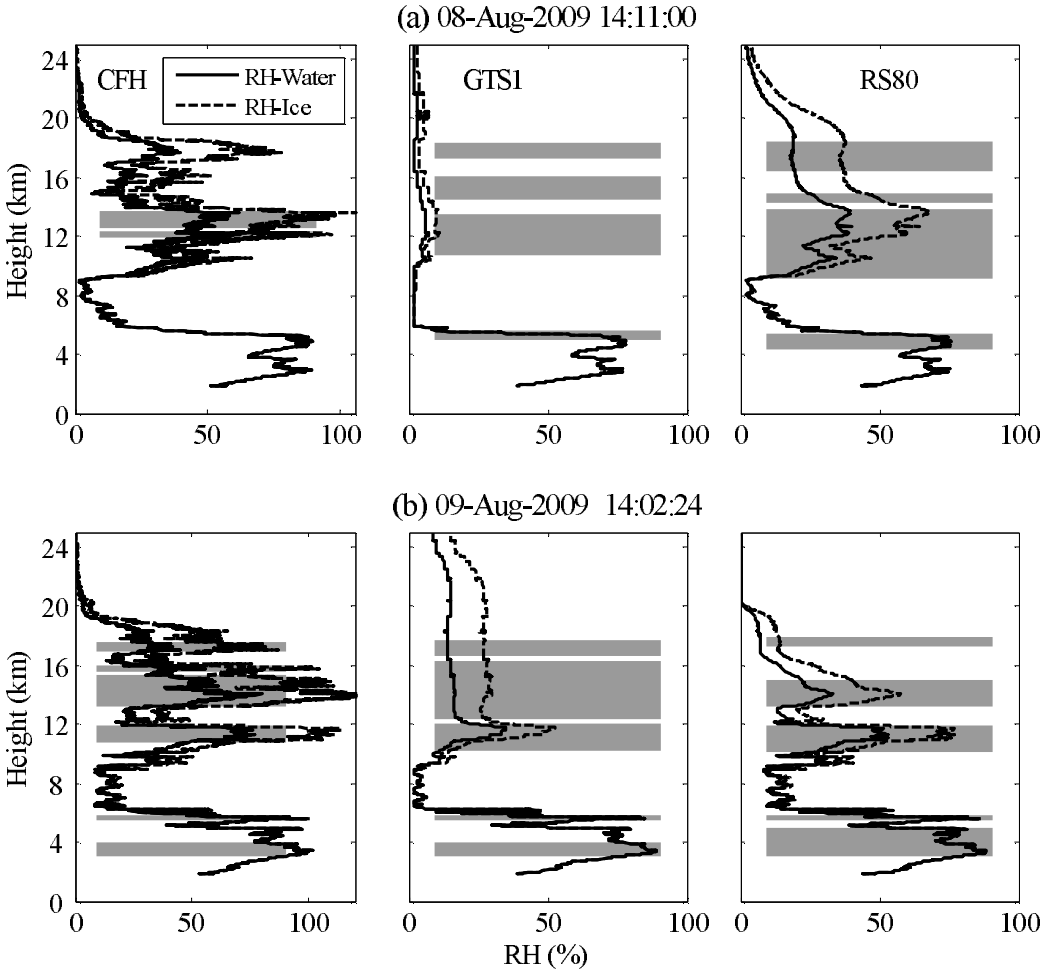

Fig. 6. Cloud layers derived from CFH, GTS1, and RS80 measurements made on (a) 8 August 2009 at 1411 LST, and (b) 9 August 2009 at 1402 LST. The solid lines represent RH with respect to water, and the dashed lines represent RH with respect to ice (temperatures $< 0^{\circ}$C).

launched on 9 August 2009 at 1402 LST, are shown in Fig. 6b. Agreement among the locations of cloud layers retrieved from the three instruments is better than that seen in Fig. 6a. A total of six, five, and five cloud layers are derived from CFH, GTS1, and RS80 measurements, respectively. Cloud distributions obtained by the three instruments are very similar, although there are some differences in the thickness of the fourth layer.

Figure 7 shows mean cloud base and/or cloud-top heights and thicknesses in different altitude ranges for cases 2–11 (Table 1). The gray area represents the location of cloud layers derived from the radiosonde. Below 5 km, mean cloud information derived from measurements taken by all three instruments are close in magnitude because RH measurements are highly accurate in this region of the atmosphere, and the method used to determine cloud layers is similar for all instruments. From 5 km to 10 km, more differences are seen among the set of three cloud layer retrievals. The number of cloud layers retrieved from GTS1 and RS80 measurements is slightly larger than that from CFH measurements, and the mean location of the CFH-derived cloud layer is generally located at an altitude that falls somewhere between the altitudes of the cloud layers derived from GTS1 and RS80 measurements. The mean cloud-layer thickness is greatest from RS80 retrievals (1687 m) and smallest from CFH retrievals (759 m). Above 10 km, cloud layer information from CFH and RS80 retrievals are similar. The mean thickness (1531 m) and total number of cloud layers (i.e., 27) is largest from GTS1 retrievals. Figure 7d shows that although the agreement among the three instrument retrievals may not be good when considering different cloud base altitude ranges, they agree reasonably well when all cloud layers are considered

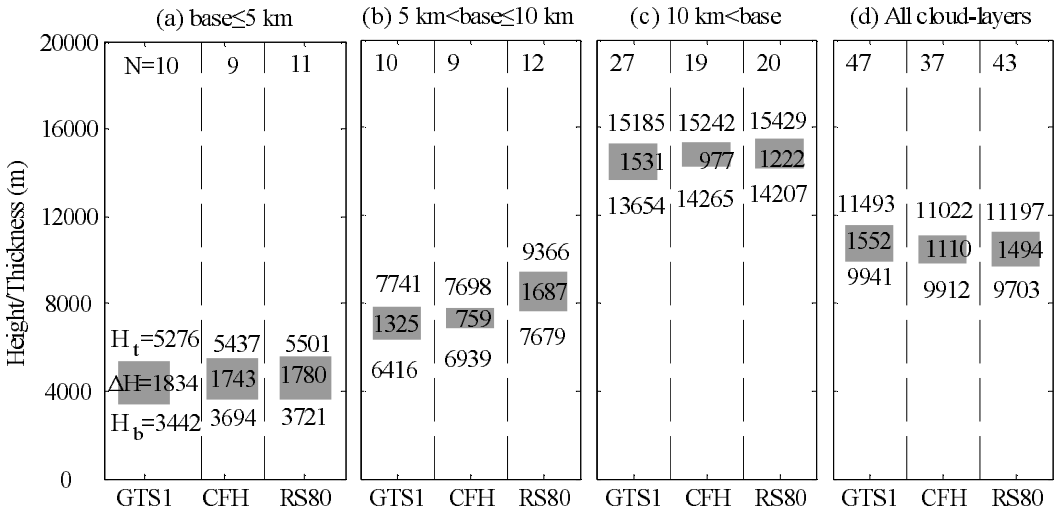

Fig. 7. Mean locations and thicknesses of cloud layers with (a) bases lower than 5 km, (b) bases ranging from 5 km to 10 km, (c) bases higher than 10 km, and (d) all cloud layers. $H_{\rm b}$, $H_{\rm t}$, and ΔH are the mean cloud-base height, mean cloud-top height, and mean thickness (units in m), respectively. N denotes the number of cloud layers. The gray area represents the location of cloud layers from the radiosonde.

together.

4. Discussion and summary

Based on radiosonde measurements made at Kunming in Yunnan province from 7 to 13 August 2009, we developed methods to determine the location of cloud layers from CFH, GTS1, and RS80 measurements. The accuracies of CFH, GTS1, and RS80 measurements changed with increase in altitude. Below 5 km, RH measurements from the three instruments had similar accuracies; above 5 km, the CFH made the most accurate measurements. Temperature measurements from the GTS1 and the RS80 were very close below 18 km; above 18 km, the temperatures from the GTS1 were higher than those from the RS80.

Taking into account the different sounding accuracies, methods for determining cloud layers were developed for each instrument, based on the methodologies of WR95 and CE96. The method for the CFH used height-resolving RH thresholds, which requires very accurate measurements of RH. Below 5 km, the methods for the GTS1 and the RS80 were similar to that of the CFH; above 5 km, the methodology of CE96 was followed using different criteria for RH thresholds.

Comparisons of cloud-layer retrievals derived from measurements made by the three instruments illustrated that they were able to provide reasonable information about the distribution of cloud layers in the atmospheric column. Below 10 km, cloud distributions derived from the three instruments were similar. Above 10 km, cloud layers derived from measurements made by the CFH were generally detected by the GTS1/RS80; however, cloud layers from the GTS1/RS80 occurred more frequently than those from the CFH. The average cloud layer locations obtained from the three cloud layer retrievals were similar, although discrepancies emerged at a detailed level.

Knowledge of cloud vertical distribution is vital for meteorological and climate studies. Such information is unavailable for most parts of the world, including the large territory of China. Although CloudSat can provide cloud vertical distribution information, its narrow nadir view limits its global sampling. The GTS1 is the operational radiosonde routinely deployed at many stations in China. Therefore, cloud vertical distributions obtained during the past ten years could be investigated by using GTS1 observations. A future study will focus on validating methods and results presented here using ground-based observations of cloud layers from remote sensing instruments.

Acknowledgements. We gratefully acknowledge the work performed by staff at the Kunming National Reference Climatological Station. We would like to thank Dr. Holger Vömel from the GRUAN Lead Center, Meteorologisches Observatorium Lindenberg, German Weather Service, Germany, for his instruction and contributions to this study. We also thank Prof. WANG Weiguo from Yunnan University and Dr. LI Peng for their work during the observation campaign. This work was supported by National Natural Science Foundation of China (Grant

No. 40830102) and the program "The Multi-scale Comprehensive Observation and Study of Spatial-Temporal Properties of Aerosol Project (MOSTap)" of National Basic Research Program of China (973 Program; Grant No. 2010CB950804).

REFERENCES

Alduchov, O. A., and E. E. Eskridge, 1996: Improved Magnus' form approximation of saturation vapor pressure. *J. Appl. Meteor.*, **35**, 601–609.

Arabey, E. N., 1975: Radiosonde data as means for cloud layers revealing cloud layer. *Meteorologiya i Gidrologiya*, **6**, 23–37. (in Russian)

AWS, 1979: The use of the skew of T, log P diagram in analysis and forecasting. Air Weather Service Tech. Rep., AWS/TR-79/006, Scott AFB, IL, 150pp.

Bian, J., 2009: Recent advances in the study of atmospheric vertical structures in upper troposphere and lower stratosphere. *Advance in Earth Science*, **24**(3), 262–271. (in Chinese)

Bian, J., H. Chen, H. Vömel, Y. Duan, Y. Xuan, and D. Lü, 2011: Intercomparison of humidity and temperature sensors: GTS1, Vaisala RS80, and CFH. *Adv. Atmos. Sci.*, **28**(1), 139–146, doi: 10.1007/s00376-010-9170-8.

Cady-Pereira, K. E., M. W. Shephard, D. D. Turner, E. J. Mlawer, S. A. Clough, and T. J. Wagner, 2008: Improved daytime column-integrated precipitable water vapor from Vaisala radiosonde humidity sensors. *J. Atmos. Oceanic Technol.*, **25**, 873–883, doi: 10.1175/2007JTECHA1027.1.

Chahine, M. T., and Coauthors, 2006: AIRS improving weather forecasting and providing new data on greenhouse gases. *Bull. Amer. Meteor. Soc.*, **87**, 911 –926.

Chen, H., J. Bian, and D. Lü, 2006: Advances and prospects in the study of stratosphere troposphere exchange. *Chinese J. Atmos. Sci.*, **30**(5), 813–820. (in Chinese)

Chernykh, I. V., 1999: Averages of relative humidity at the cloud base level. WMO report, No. 28, WMO/TD 942, 2.7–2.8.

Chernykh, I. V., and R. E. Eskridge, 1996: Determination of cloud amount and level from radiosonde soundings. *J. Appl. Meteor.*, **35**, 1362–1369.

Chernykh, I. V., and O. A. Alduchov, 2000: Comparison of cloud layers detecting by different methods. *Proc. Fifth International Cloud Modeling Workshop*, Colorado, USA, 1–22.

Chernykh, I. V., O. A. Alduchov, and R. E. Eskridge, 2000: Trends in low and high cloud boundaries and errors in height determination of cloud boundaries. *Bull. Amer. Meteor. Soc.*, **82**(9), 1941–1947.

Dolgin, M. I., 1983: Determine scheme clouds from atmosphere sounding in Antarctic Continent. *Meteorologiya i Gidrologiya*, **11**, 47–51. (in Russian)

Han, D., and R. G. Ellingson, 2000: An experimental technique for testing the validity of cumulus cloud parameterizations for longwave radiation calculations. *J. Appl. Meteor.*, **39**, 1147–1159.

Hyland, R. W., and A. Wexler, 1983: Formulations for the thermodynamic properties of the saturated phases of H_2O from 173.15 K to 473.15 K. *ASHRAE Transactions*, **89**(2A), 500–519.

Li, F., 2006: New developments with upper-air sounding in China. Instruments and Observing Methods Report No. 94, WMO/TD No.1354, WMO, Geneva, 9pp.

Li, W., F. Li, Z. Zhao, F. Liu, B. Li, and H. Li, 2009: *Technical Assessment Report of L-band Upper Air Sounding System*. China Meteorological Press, Beijing, 95pp. (in Chinese)

Miloshevich, L. M., H. Vömel, A. Paukkunen, A. J. Heymsfield, and S. J. Oltmans, 2001: Characterization and correction of relative humidity measurements from Vaisala RS80-A radiosondes at cold temperatures. *J. Atmos. Oceanic Technol.*, **18**, 135–155.

Miloshevich, L. M., A. Paukkunen, H. Vömel, and S. J. Oltmans, 2004: Development and validation of a time lag correction for Vaisala radiosonde humidity measurements. *J. Atmos. Oceanic Technol.*, **21**, 1305–1327.

Miloshevich, L. M., H. Vömel, D. N. Whiteman, B. M. Lesht, F. J. Schmidlin, and F. Russo, 2006: Absolute accuracy of water vapor measurements from six operational radiosonde types launched during AWEX-G and implications for AIRS validation. *J. Geophys. Res.*, **111**, D09S10, doi: 10.1029/2005JD006083.

Miloshevich, L. M., H. Vömel, D. N. Whiteman, and T. Leblanc, 2009: Accuracy assessment and correction of Vaisala RS92 radiosonde water vapor measurements. *J. Geophys. Res.*, **114**, D11305, doi: 10.1029/2008JD011565.

Minnis, P., Y. Yi, J. Huang, and J. K. Ayers, 2005: Relationships between radiosonde and RUC-2 meteorological conditions and cloud occurrence determined from ARM data. *J. Geophys. Res.*, **110**, D23204, doi: 10.1029/2005JD006005.

Naud, C., J. P. Muller, and E. E. Clothiaux, 2003: Comparison between active sensor and radiosonde cloud boundaries over the ARM Southern Great Plains site. *J. Geophys. Res.*, **108** (D4), 4140, doi: 10.1029/2002JD002887.

Poore, K. D., J. Wang, and W. Rossow, 1995: Cloud layer thickness from a combination of surface and upper-air observations. *J. Climate*, **8**, 550–568.

Slingo, J. M., 1980: A cloud parameterization scheme derived from GATE data for use with a numerical model. *Quart. J. Roy. Meteor. Soc.*, **106**, 747–770.

Soden, B. J., D. D. Turner, B. M. Lesht, and L. M. Miloshevich, 2004: An analysis of satellite, radiosonde, and lidar observations of upper tropospheric water vapor from the Atmospheric Radiation Measurement program. *J. Geophys. Res.*, **109**, D04105, doi: 10.1029/2003JD003828.

Turner, D. D., B. M. Lesht, S. A. Clough, J. C. Liljegren, H. E. Revercomb, and D. C. Tobin, 2003: Dry bias

and variability in Vaisala RS80-H radiosondes: The ARM experience. *J. Atmos. Oceanic Technol.*, **20**, 117–132.

Vömel, H., D. E. David, and K. Smith, 2007a: Accuracy of tropospheric and stratospheric water vapor measurements by the cryogenic frost point hygrometer: Instrumental details and observations. *J. Geophys. Res.*, **112**, D08305, doi: 10.1029/2006JD007224.

Vömel, H., and Coauthors, 2007b: Radiation dry bias of the Vaisala RS92 humidity sensor. *J. Atmos. Oceanic Technol.*, **24**, 953–963.

Wang, J., 1997: Determination of cloud vertical structure from upper air observations and its effects on atmospheric circulation in a GCM. Ph.D. dissertation. Columbia University, 233pp.

Wang, J., and W. B. Rossow, 1995: Determination of cloud vertical structure from upper-air observations. *J. Appl. Meteor.*, **34**, 2243–2258.

Wang, J., W. B. Rossow, T. Uttal, and M. Rozendaal, 1999: Variability of cloud vertical structure during ASTEX observed from a combination of rawinsonde, radar, ceilometer, and satellite. *Mon. Wea. Rev.*, **127**, 2482–2502.

Wang, J., H. L. Cole, D. J. Carlson, E. R. Miller, K. Beierle, A. Paukkunen, and T. K. Laine, 2002: Corrections of humidity measurement errors from the Vaisala RS80 radiosonde—Application to TOGA COARE data. *J. Atmos. Oceanic Technol.*, **19**, 981–1002.

Wang, J., D. J. Carlson, D. B. Parsons, T. F. Hock, D. Lauritsen, H. L. Cole, K. Beierle, and E. Chamberlain, 2003: Performance of operational radiosonde humidity sensors in direct comparison with a chilled mirror dew-point hygrometer and its climate implication. *Geophys. Res. Lett.,* **30**(16), 1860, doi: 10.1029/2003GL016985.

Wang, Z., and Y. Sheng, 1991: The new method of deriving cloud parameters from radiosonde data. *Education and Science and Technology of Meteorology*, **1**, 18–21. (in Chinese)

Xu, W., 2006: Carbon humidity sensor of GTS Radiosonde performance testing results and its application. M. S. thesis, Chinese Academy of Meteorological Sciences, 64pp. (in Chinese)

Yao, W., Y. Ma, and W. Xu, 2008: Relative humidity error of L-band electronic radiosonde and its application. *Journal of Applied Meteorological Science*, **19** (3), 356–361. (in Chinese)

Zhang, J., H. Chen, Z. Li, X. Fan, L. Peng, Y. Yu, and M. Cribb, 2010: Analysis of cloud layer structure in Shouxian, China using RS92 radiosonde aided by 95 GHz cloud radar. *J. Geophys. Res.*, **115**, D00K30, doi: 10.1029/2010JD014030.